Published in final edited form as:

Biotech Histochem. 2019 February ; 94(2): 134–144. doi:10.1080/10520295.2018.1530373.

Impact of tissue preservation on collagen fiber architecture

HN Hutson[1], **C Kujawa**[1], **K Eliceiri**[1,2], **P Campagnola**[1], and **KS Masters**[1]

[1]Department of Biomedical Engineering, University of Wisconsin-Madison, Madison, Wisconsin, USA

[2]Laboratory for Optical and Computational Instrumentation, Laboratory of Cell and Molecular Biology, University of Wisconsin-Madison, Madison, Wisconsin, USA

Abstract

Microarchitectural features of collagen-rich extracellular matrices provide the mechanical foundation for tissue function and exhibit topographical cues that influence cellular behavior including proliferation, migration and protein expression. Preservation of tissue microarchitecture is required for accurate evaluation of tissue characteristics and pathology. It is unclear whether common tissue preservation methods possess equal ability to preserve microarchitecture. We investigated collagen microarchitecture in samples that had been flash frozen, fixed in formalin or preserved in RNA*later®*, and which contained both collagen-rich and collagen-sparse regions. Fibrillar collagen organization was characterized using picrosirius red staining and second harmonic generation (SHG) microscopy. Maintenance of collagen fiber characteristics compared to the gold standard of flash freezing depended on both the method of preservation and the local collagen content of the tissue. Both formalin fixation and RNA*later®* preserved collagen fiber characteristics similar to flash freezing in collagen-rich areas of the tissue, but not in collagen-sparse regions. Analysis using picrosirius red staining indicated preservation-dependent changes in overall tissue architecture and suprafibrillar organization. Together with considerations of cost, ease of use, storage conditions and ability to use the preserved tissue for RNA or protein analysis, our quantitative characterization of the effects of preservation method on collagen microarchitecture may help investigators select the most appropriate preservation approach for their needs.

Keywords

collagen; heart valve; imaging; microarchitecture; picrosirius red; RNA*later*®; tissue preservation

An optimal approach to tissue preservation must balance many factors including cost, ease of use and storage, storage longevity, ability to multiplex tissue analysis, and retention of native tissue structure and physiology. Flash freezing (snap freezing) of tissues in liquid nitrogen often is considered the “gold standard” for tissue preservation owing to its ability to

Contact: Kristyn S. Masters, PhD, Department of Biomedical Engineering, 1111 Highland Ave, 8531 WIMR II, Madison, WI 53705, kmasters@wisc.edu, Phone: (608) 265-4052, Fax: (608) 263-9239.

Declaration of interest

The authors declare no conflicts of interest.

preserve native tissue structure and the integrity of nucleic acids and phosphoproteins (Beckstead 1994; Mueller et al. 2011; Kashofer et al. 2013; Staff et al. 2013). Despite the benefits of flash freezing, however, the technique requires access to liquid nitrogen immediately following tissue isolation and continued storage of banked tissues at temperatures ≤ −20° C, which renders it costly and impractical for large scale tissue acquisition and storage (Cox et al. 2006).

Formalin fixation is the standard technique for long term tissue preservation, because it overcomes many of the difficulties associated with flash freezing while preserving tissue morphology (Dotti et al. 2010). Formalin fixation enables facile sample collection, temporary storage at room temperature and simple transportation between tissue isolation and storage sites (Bussolati et al. 2011). Formalin fixation, however, causes nucleic acid fragmentation and decreases RNA extraction efficiency owing to the creation of crosslinks (Williams et al. 1999; Cronin et al. 2004; von Ahlfen et al. 2007; David et al. 2011). The crosslinking of proteins in the preserved tissue occurs by formation of methylene bridges (Buesa 2008; Howat and Wilson 2014), which interferes with the integrity of phosphoproteins and necessitates the use of heat or other methods to reduce the crosslinks prior to RNA isolation or immunohistochemistry (Mueller et al. 2011; Neumeister 2014).

RNA*later®* is an ammonium sulfate solution; it is used infrequently for histological preparations, but has been widely used to stabilize nucleic acids in tissue samples for subsequent gene expression or genomic analysis (Florell et al. 2001). Previous studies have shown that tissues stored in RNA*later®* yield comparable (Bennike et al. 2016) or even better RNA quality than flash frozen tissues (Hatzis et al. 2010; Sherker et al. 2013). Tissue banks also have begun adopting RNA*later®* storage protocols owing to its greater ability to preserve nucleic acid integrity compared to formalin fixed samples, while producing similar histological results (Florell et al. 2001). The ability to use a single sample for different types of analysis is desirable due to limited tissue availability, which is a common and significant obstacle for analysis of both human and animal specimens (Gugic et al. 2007; Lin et al. 2009).

Although the approaches to tissue preservation described above have been compared extensively with respect to histological, immunohistochemical and gene expression (Beckstead 1994; Su et al. 2004), the effect of the preservation method on tissue microarchitecture has received less attention (Schenke-Layland et al. 2007). Appreciation is increasing for the importance of collagen fiber architecture in determining cell behavior (Muthusubramaniam et al. 2012; Fraley et al. 2015), disease progression (Provenzano et al. 2008; Drifka et al. 2016) and mechanical properties (Sacks et al. 1998; Hadi and Barocas 2013). It is imperative to preserve these structures faithfully during sample preservation to enable accurate analysis of tissue pathobiology (Lee et al. 2005; Fraley et al. 2015).

We investigated two common methods for collagen detection, the histological stain, picrosirius red (Lattouf et al. 2014) and the label free imaging method of second harmonic generation (SHG) imaging (Campagnola et al. 2001). These two imaging methods were used to evaluate how different preservation methods altered the collagen fiber architecture of two

model tissues: one that exhibits distinct high density and low density collagen areas within the same native tissue structure and one that exhibits a high degree of collagen crimping.

We examined and quantified the collagen fiber structure of porcine aortic heart valves, which exhibit a distinct trilaminar architecture comprising a region of high collagen content and alignment (fibrosa), a region of low collagen content and high glycosaminoglycan content (spongiosa) and a region of significant elastin content (ventricularis) (Stella and Sacks 2007; Schoen and Gotlieb 2016). The thin nature of the valve also ensures rapid and complete penetration of preservation solutions, which minimizes differences in diffusion of the solutions through the tissue (Buesa 2008). We also analyzed collagen architecture in rat tail tendon fascicles (RTTfs), which have a dense and crimped collagen structure and are often used as a standard for SHG imaging (Freund et al. 1986; Campagnola and Loew 2003; Williams et al. 2005). We characterized and quantified the effect of different preservation methods on collagen microarchitecture. Added to what is known about the limitations and advantages of these preservation techniques, our findings may provide further guidance to investigators for selecting the most appropriate preservation method for their needs.

Material and methods

All materials were purchased from Sigma Aldrich (St. Louis, MO) unless otherwise noted.

Tissue acquisition and preservation

Aortic heart valves were excised from hearts of 5- and 6-month-old pigs obtained from a local butcher (Hoesly's Meats, New Glarus, WI). Rat tails were collected from rats undergoing euthanasia for other studies and tendon fascicles were removed. Valve leaflets and RTTfs were isolated within 4 h of animal slaughter and washed in phosphate-buffered saline (PBS) before preservation using one of three methods. "Frozen" denotes tissues that were flash frozen in liquid nitrogen and stored at −20° C until embedment in paraffin. The other two preservation methods required treatment with exogenous chemicals: "formalin" refers to tissues fixed in 10% neutral buffered formalin for at least 24 h and "RNA*later*®" refers to tissues preserved by immersion in RNA*later*® for at least 24 h. Tissues preserved in formalin or RNA*later*® were stored at −20° C in their respective preservation solutions until paraffin embedment.

Histological staining

Tissues were washed in fresh PBS, then flash frozen using liquid nitrogen, stored in 10% formalin or stored in RNA*later*® before preparation for staining. Fascicles were cut to fit within the mounting area of the slide (approximately 3 cm) and washed prior to histological staining. Heart valve leaflets were dehydrated through 70, 80, 95 and 100% ethanol, cleared in xylene, and embedded in paraffin. Sections were cut at 5 μm and mounted on glass slides. The sections then were deparaffinized using xylene substitute, rehydrated through 100, 95, 70 and 50% ethanol and rinsed in water prior to staining with picrosirius red to visualize collagen as described previously (Puchtler et al. 1973; Dayan et al. 1989). Briefly, tissue sections were stained using 0.1 % (w/v) direct red 80 (CI 35780) in saturated aqueous picric acid solution for 1 h. Excess stain solution was removed before tissues were washed twice in

acidified water, dehydrated through three washes with 100% ethanol, cleared in xylene substitute and mounted with Permount. Sections were imaged using an Olympus BX60 upright microscope (Olympus, Tokyo, Japan) with a DP25 camera using cellSens Standard software (V1.13) for both bright field and linearly polarized birefringence. The birefringence of three areas of equal dimensions/tissue layer/image was measured using FIJI (an open-source variant of ImageJ, version 2.0.0-rc-43/1.5e) (Schindelin et al. 2015). The birefringence of each region of interest was analyzed using the method described by Rich and Whittaker (2005) to quantify the percentage of tissue area that exhibited birefringence and the distribution of the birefringence. Briefly, three equal areas/image were selected from within each heart valve layer. Images were converted to 8-bit color images before analysis. Because birefringence appears as non-black hues using this method, total birefringence was calculated as the total non-black area, in pixels, within the selected area. Distribution of birefringence was calculated as the percentage of the non-black area that fell within hue thresholds for red (2–9 and 230–256), orange (10–38), yellow (39–51) and green (52–128). Tissue width and crimp period were analyzed in RTTfs, because these are standard measurements for these tissues (Williams et al. 2005). Width was measured at five locations/image along the fascicle. Crimp period was the distance measured between areas of minimum birefringence along the length of the RTTfs. The crimp period was measured at five places in each image and averaged/image for further analysis.

SHG imaging and collagen fiber analysis

Paraffin embedded valves were cut into 13–15 μm thick sections for detection of collagen by SHG imaging. SHG exploits the ability of fibrillar collagen to generate a second harmonic wave at 445 nm to provide detailed micro-level structural information without staining or chemical treatment. Deparaffinized tissues were rehydrated as described above before mounting with coverslips, then sealed with lacquer. Fascicles were cut to fit within the mounting area of the slide (approximately 3 cm) and washed before mounting and sealing. Sections were stored at 4° C and imaged within 2 weeks. SHG imaging was conducted using an Olympus BX61 upright microscope (Olympus) with an Olympus Fluoview 300 scanning system at 2 × digital zoom to satisfy the Nyquist sampling criterion. Excitation was provided by a mode-locked 890 nm laser (Coherent Santa Clara, CA) with excitation by a 40 × water immersion objective (working distance 3 mm, 0.8 NA). The forward signal was collected with a 0.9 NA condenser and isolated with a 445/20 nm bandpass filter (Semrock, Rochester, NY).

We analyzed fiber characteristics in three tissue sections of valve leaflets in three distinct areas of each section. SHG was collected throughout the depth of the tissue section at a step size of 1 μm and the five middle images were averaged for analysis. SHG was not collected from the ventricularis layer of the valve leaflets, because the organization of the fibers within that layer are perpendicular to the field of view and the layer is too thin to be visualized by *en face* sectioning. Analysis of RTTfs fiber characteristics was conducted in a manner similar to analysis of valve leaflets, with SHG collected through the entire depth of three distinct fascicles and in three distinct areas of each fascicle.

We quantified fiber characteristics using CT-FIRE V2 Beta and CurveAlign V4.0 Beta (Liu et al. 2017), which are open source software programs developed by the Laboratory for Optical and Computational Instrumentation (LOCI) at the University of Wisconsin-Madison. SHG images in 8-bit tiff format were imported into the program where they were subjected to curvelet transform (CT) reconstruction using CurveLab 2.1.2 (April 2008) followed by creation of fiber overlays using the FIRE algorithm. The fiber outputs from CT-FIRE then were subjected to feature analysis using CurveAlign for output of final fiber features. MATLAB (The MathWorks, Inc., Natick, MA) was used as the platform to run the CT-FIRE and CurveAlign software. Data from selected fibers then were exported from CurveAlign into Excel (Microsoft, Redmond, WA) for statistical analysis.

Quantification of multiple fiber characteristics was reported using the following definitions: “fiber width” is the width at multiple points along the fiber within the image; “distance to nearest x,” where x is either 2, 4, 8 or 16 fibers, is the distance in microns between the nearest x fibers from multiple points along the length of the reference fiber; “box density” is measurement of the average number of fibers within a region of specified size; “fiber angle” denotes the average angle of fibers within an image relative to each other; “alignment of nearest x,” where x is either 2, 4, 8 or 16 fibers, is a measurement of the alignment of the nearest x fibers relative to a reference fiber where 0 indicates no alignment, or the fibers are perpendicular and 1 indicates complete alignment where the fibers are parallel; “box alignment” is a measurement of the alignment of all fibers within an area of specified size, with 0 indicating no alignment and 1 indicating complete alignment of fibers within the region.

Statistical analysis

Statistical analysis of data from SHG imaging was performed using Prism 6 (GraphPad Software, Inc., La Jolla, CA) with one-way ANOVA and Tukey’s *post hoc* test. Statistical significance of all other groups was analyzed using a two-tailed, unpaired t-test assuming equal variance. For all tests, n = 3 unless otherwise noted. Values for $p \leq 0.05$ were considered significant.

Results

Collagen architecture assessed by picrosirius red birefringence

The impact of tissue preservation technique on collagen organization was examined first using linearly polarized light imaging of heart valve leaflet sections stained with picrosirius red. This approach provides semiquantitative information about both the fraction of tissue that is composed of fibrillar collagen, i.e., the percentage of total tissue area that exhibits birefringence, as well as the diameter of the fibers. Figure 1A shows bright field images of leaflet sections stained with picrosirius red, where areas of fibrillar collagen are indicated by red staining. Corresponding images of picrosirius red birefringence are shown in Figure 1B, where fiber diameter is indicated by the color of birefringence; thin fibers appear green, and yellow, orange and red indicate increasing thickness. As expected in a normal aortic valve leaflet, the fibrosa was dense with collagen, while the spongiosa (middle) was more sparsely populated with collagen fibers. The percentage of total area that exhibited birefringence

within the fibrosa was not significantly different among the three preservation methods (Figure 2A). In the spongiosa, the fraction of tissue composed of fibrillar collagen also was similar among all preservation methods. As expected, the collagen content within the spongiosa was generally less than that observed in the fibrosa (Figure 2B).

Sections of valve leaflet stained with picrosirius red also were analyzed to determine the percentage of total birefringence represented by each hue: green, yellow, orange or red. The amount of red birefringence in the fibrosa did not differ among tissues that had been fixed in formalin compared to those that had been flash frozen ($p = 0.08$), but the fibrosa of tissues preserved in RNA*later®* exhibited significantly less red birefringence compared to both frozen and formalin fixed tissues ($p = 0.017$ and 0.049, respectively) (Figure 2C). The amount of orange birefringence in the fibrosa of tissues preserved in RNA*later®* was similar to that observed in frozen tissues, but was significantly greater than the orange birefringence in the fibrosa of tissues preserved in formalin ($p = 0.0010$). Analysis of each hue as a percentage of total birefringence in the spongiosa produced similar findings (Figure 2D), but preservation in RNA*later®* produced decreased red and orange birefringence compared to frozen tissues ($p = 0.0016$ and 0.00036 for red and orange, respectively) and formalin fixed tissues ($p = 0.041$ and 0.013, respectively). No significant difference was observed between formalin fixed and frozen tissues for any birefringence analysis.

Fascicles stained with picrosirius red were analyzed for crimp period and fascicle width to investigate the impact of preservation methods on characteristics related to rat tendon fascicle functions such as contraction (Figure 3) (Lavagnino et al. 2017). Analysis of RTTf width revealed significant differences among preservation techniques (Figure 3C). Formalin fixation caused decreased width compared to frozen RTTfs ($p = 0.030$), which is consistent with previous reports (Williams et al. 2005). The width of fascicles preserved in RNA*later®* was similar to tissues that had been flash frozen, but they were significantly wider compared to formalin fixed fascicles ($p = 0.010$). Fascicles preserved in formalin had a significantly longer crimp period than frozen tissues ($p = 0.014$), but the crimp period of fascicles preserved in RNA*later®* did not differ significantly compared to RTTfs that were flash frozen or preserved in formalin ($p = 0.073$ and 0.19, respectively) (Figure 3D).

Assessment of collagen architecture by SHG imaging

Picrosirius red birefringence provided information about collagen localization and organization in the preserved tissues and some insight into the suprafibrillar architecture of RTTFs, e.g., crimping. Further analysis of individual fiber characteristics was required to understand the effects of the preservation methods on collagen architecture. Therefore, we performed SHG imaging of valve leaflet sections (Figure 4) and RTTfs (Figure 5) to determine whether the preservation method affected the characteristics of individual collagen fibers and their organization relative to neighboring fibers.

In the collagen-dense fibrosa layer of the leaflet, SHG analysis exhibited consistent values for virtually all fiber characteristics measured, including fiber width, density and alignment, among all three preservation techniques (Table 1). We found some preservation-dependent variation in fiber characteristics in the spongiosa, the collagen-sparse layer of the valve leaflet. Although fiber width in the spongiosa was consistent among all preservation

methods, fixation in formalin increased the distance between individual fibers compared to flash frozen samples; however, the overall fiber density among larger tissue areas remained similar for all preservation methods. In collagen-sparse regions, fiber alignment was most consistently altered by preservation method; both RNA*later*® and formalin produced lower alignment values compared to the flash frozen preservation (Table 2).

We conducted SHG analysis of collagen fibers on RTTfs. Despite the preservation-dependent differences in fascicle width and crimp period observed for picrosirius red analysis, no significant differences were observed in fiber width, density or alignment measurements among all preservation methods using SHG analysis (Table 3).

Discussion

Microarchitectural features of the extracellular matrix (ECM) provide topographical cues that influence many cellular behaviors including protein expression, proliferation, differentiation and migration (Provenzano et al. 2008; Cox and Erler 2011; Riching et al. 2014). Fibrillar collagen is the dominant microstructural element and the most abundant component of ECM in the body. Changes in collagen fiber features can be important indicators of tissue health or disease prognosis. For example, hypertrophic cardiomyopathy is associated with a significant increase in collagen fiber size (Shirani et al. 2000), while alignment of collagen fibers is thought to be a predictor of breast tumor metastasis and patient survival (Provenzano et al. 2006; Conklin et al. 2011).

To enable accurate investigation of tissue function and pathology, it is critical to ensure that tissue preparation preserves microstructure faithfully. We found that both formalin and RNA*later*® maintained the collagen fiber architecture of collagen-dense areas as evaluated by SHG imaging. The method of preservation, however, affected some aspects of fiber arrangement in collagen-sparse areas of tissues.

We investigated the preservation of the trilayer structure of the aortic heart valve by analyzing collagen architecture using both histological and advanced imaging techniques. Heart valve leaflets and RTTfs preserved in either RNA*later*® or formalin generally exhibited tissue morphology similar to frozen tissues. Birefringence hue distribution following preservation in RNA*later*®, however, differed from both flash frozen or formalin fixed tissues. Because birefringence results from multiple interactions of the picrosirius red dye with collagen, the change in red and orange birefringence associated with RNA*later*® preservation could indicate a shift in either fiber density or width (Junqueira et al. 1982; Dayan et al. 1989). Therefore, to quantify more definitively and to compare fiber features under different conditions, we employed SHG to analyze collagen fiber architecture following the different tissue preservation methods.

Analysis of collagen microarchitecture using SHG demonstrated that all three preservation methods were equivalent in their ability to preserve the width of collagen fibers throughout the collagen-rich and collagen-sparse areas of the aortic valve. Compared to frozen tissues, both RNA*later*® and formalin preservation also preserved the density and alignment of collagen fibers in collagen-rich areas. The latter observation is consistent with earlier reports

of comparing fibrillar collagen organization between flash frozen and formalin fixed tissues (Pena et al. 2007; Chen et al. 2011); these investigators did not include RNA*later®* and limited their study to qualitative observations of ECM structure. We found that in collagen-sparse areas, many measures of alignment, e.g., degree of alignment with nearest x fibers or overall fiber alignment within an area of specified dimensions, were significantly lower for tissues preserved in RNA*later®* or formalin compared to flash frozen tissue. We did not observe this difference in alignment features for RTTfs preserved in formalin or RNA*later®*, which suggests that the effects of the preservation method on alignment may be specific to local collagen sparseness. Also, the differences in collagen fiber density and/or width implied by the birefringent hue analysis of tissues preserved in RNA*later®* vs. flash frozen were not corroborated by the more precise fiber analysis using SHG. The discrepancy between birefringence and SHG analysis may be due to an artifact caused by inadvertent fixation of the tissue by the alcohol that is used during histological processing (Montes and Junqueira 1991). Alcohol fixation could cause frozen tissues and tissues preserved in RNA*later®* to exhibit differences in birefringence compared to tissues that had been formalin fixed prior to processing (Jarrett and Hardy 1957; Dapson 1993).

Our findings provide valuable information about the preservation of the ECM structure for both histological and advanced imaging techniques, but we focused solely on fibrillar collagen architecture and did not address other ECM components. Although our findings indicate little impact of preservation method on collagen fiber measurements, it is possible that the method of preservation could impact the nano- or microscale architecture of other ECM components. We also did not investigate the ability of these preservation methods to preserve nucleic acids or phosphoproteins, because this outcome has been described in detail elsewhere (Florell et al. 2001).

Preservation of tissue by either RNA*later®* or formalin conserved native tissue microarchitecture comparably to the standard of flash freezing. Therefore, any of the preservation methods discussed here could be used to preserve the microarchitectural features of the extracellular matrix and therefore are valuable methods for preserving tissues for investigation of architectural characteristics of tissues. RNA*later®* may offer improved versatility compared to other common methods by combining many of the advantages of formalin fixation, e.g., ease of use and handling, with those of flash freezing, e.g., nucleic acid preservation (Sherker et al. 2013), while also preserving equivalent architecture. Our findings corroborate an earlier recommendation to use RNA*later®* as an alternative to formalin for tissue banking (Florell et al. 2001). Our findings also indicate that samples preserved using different methods, e.g., formalin and RNA*later®*, should not be combined when performing histological analysis. Although neither formalin nor RNA*later®* introduced significant departure from flash freezing results in terms of fiber architecture in collagen-rich areas, they did exhibit differences in areas of sparse collagen.

Our findings may be considered together with cost, ease of use, storage conditions and ability to use the preserved tissue for RNA or protein analysis to help guide investigators in their selection of preservation methods that are most appropriate for their specific needs

Acknowledgments

Funding

Our work was supported by the National Heart, Lung, and Blood Institute and the National Institute of Biomedical Imaging and Bioengineering at the National Institutes of Health (R01-HL093281 and R21-EB019508 to K.S.M.), as well as the Translational Cardiovascular Sciences Training Program (T32 HL07936) and the National Science Foundation Graduate Research Fellowship Program.

References

Beckstead JH (1994). A simple technique for preservation of fixation-sensitive antigens in paraffin-embedded tissues. J.Histochem. Cytochem 42: 1127–1134. [PubMed: 8027531]

Bennike TB, Kastaniegaard K, Padurariu S, Gaihede M, Birkelund S, Andersen V and Stensballe A (2016). Proteome stability analysis of snap frozen, RNA*later* preserved, and formalin-fixed paraffin-embedded human colon mucosal biopsies. Data .Brief 6: 942–947. [PubMed: 26937473]

Buesa RJ (2008). Histology without formalin? Ann. Diagn. Pathol 12: 387–396. [PubMed: 18995201]

Bussolati G, Annaratone L, Medico E, D'Armento G and Sapino A (2011). Formalin fixation at low temperature better preserves nucleic acid integrity. PLoS ONE 6.

Campagnola PJ, Clark HA, Mohler WA, Lewis A and Loew LM (2001). Second-harmonic imaging microscopy of living cells. J Biomed Opt 6: 277–286. [PubMed: 11516317]

Campagnola PJ and Loew LM (2003). Second-harmonic imaging microscopy for visualizing biomolecular arrays in cells, tissues and organisms. Nature Biotechnol 21: 1356–1360. [PubMed: 14595363]

Chen ACH, McNeilly C, Liu APY, Flaim CJ, Cuttle L, Kendall M, Kimble RM, Shimizu H and McMillan JR (2011). Second harmonic generation and multiphoton microscopic detection of collagen without the need for species specific antibodies. Burns 37: 1001–1009. [PubMed: 21501931]

Conklin MW, Eickhoff JC, Riching KM, Pehlke CA, Eliceiri KW, Provenzano PP, Friedl A and Keely PJ (2011). Aligned collagen is a prognostic signature for survival in human breast carcinoma. Am. J. Pathol 178: 1221–1232. [PubMed: 21356373]

Cox ML, Schray CL, Luster CN, Stewart ZS, Korytko PJ, Khan KNM, Paulauskis JD and Dunstan RW (2006). Assessment of fixatives, fixation, and tissue processing on morphology and RNA integrity. Exp. Molec. Pathol 80: 183–191. [PubMed: 16332367]

Cox TR and Erler JT (2011). Remodeling and homeostasis of the extracellular matrix: implications for fibrotic diseases and cancer. Dis. Models Mech 4: 165–178.

Cronin M, Pho M, Dutta D, Stephans JC, Shak S, Kiefer MC, Esteban JM and Baker JB (2004). Measurement of gene expression in archival paraffin-embedded tissues: development and performance of a 92-gene reverse transcriptase-polymerase chain reaction assay. Am J. Pathol 164: 35–42. [PubMed: 14695316]

Dapson RW (1993). Fixation for the 1990's: a review of needs and accomplishments. Biotech. Histochem 68: 75–82. [PubMed: 8494954]

David LE, Fowler CB, Cunningham BR, Mason JT and O'Leary TJ (2011). The effect of formaldehyde fixation on RNA: optimization of formaldehyde adduct removal. J. Molec. Diagn 13: 282–288. [PubMed: 21497290]

Dayan D, Hiss Y, Hirshberg a, Bubis JJ and Wolman M (1989). Are the polarization colors of picrosirius red-stained collagen determined only by the diameter of the fibers? Histochemistry 93: 27–29. [PubMed: 2482274]

Dotti I, Bonin S, Basili G, Nardon E, Balani A, Siracusano S, Zanconati F, Palmisano S, De Manzini N and Stanta G (2010). Effects of formalin, methacarn, and fineFIX fixatives on RNA preservation. Diagn. Molec. Pathol 19: 112–122. [PubMed: 20502189]

Drifka CR, Loeffler AG, Mathewson K, Keikhosravi A, Eickhoff JC, Liu Y, Weber SM, Kao WJ and Eliceiri KW (2016). Highly aligned stromal collagen is a negative prognostic factor following pancreatic ductal adenocarcinoma resection. Oncotarget 7: 76197–76213. [PubMed: 27776346]

Florell SR, Coffin CM, Holden Ja, Zimmermann JW, Gerwels JW, Summers BK, Jones DA and Leachman SA (2001). Preservation of RNA for functional genomic studies: a multidisciplinary tumor bank protocol. Mod. Pathol 14: 116–128. [PubMed: 11235903]

Fraley SI, Wu P-H, He L, Feng Y, Krisnamurthy R, Longmore GD and Wirtz D (2015). Three-dimensional matrix fiber alignment modulates cell migration and MT1-MMP utility by spatially and temporally directing protrusions. Sci. Rep. 5: 14580. [PubMed: 26423227]

Freund I, Deutsch M and Sprecher A (1986). Connective tissue polarity. Optical second-harmonic microscopy, crossed-beam summation, and small-angle scattering in rat-tail tendon. Biophys. J 50: 693–712. [PubMed: 3779007]

Gugic D, Nassiri M, Nadji M, Morales A and Vincek V (2007). Novel tissue preservative and tissue fixative for comparative pathology and animal research. J. Exp. Anim. Sci 43: 271–281.

Hadi MF and Barocas VH (2013). Microscale fiber network alignment affects macroscale failure behavior in simulated collagen tissue analogs. J. Biomech. Eng 135: 021026. [PubMed: 23445071]

Hatzis C, Sun H, Yao H, Hubbard RE, Meric-Bernstam F, Babiera GV, Wu Y, Pusztai L and Symmans WF (2010). Effects of tissue handling on rna integrity and microarray measurements from resected breast cancers. J. Natl. Cancer Inst 103: 1871–1883.

Howat WJ and Wilson BA (2014). Tissue fixation and the effect of molecular fixatives on downstream staining procedures. Methods 70: 12–19. [PubMed: 24561827]

Jarrett A and Hardy JA (1957). The value of alcohol for fixation of skin. Stain Technol 32: 225–233. [PubMed: 13467511]

Junqueira LC, Montes GS and Sanchez EM (1982). The influence of tissue section thickness on the study of collagen by the picrosirius-polarization method. Histochemistry 74: 153–156. [PubMed: 7085347]

Kashofer K, Viertler C, Pichler M and Zatloukal K (2013). Quality Control of rna preservation and extraction from paraffin-embedded tissue: implications for RT-PCR and microarray analysis. PLoS ONE 8.

Lattouf R, Younes R, Lutomski D, Naaman N, Godeau G, Senni K and Changotade S (2014). Picrosirius red staining: a useful tool to appraise collagen networks in normal and pathological tissues. J Histochem Cytochem 62: 751–758. [PubMed: 25023614]

Lavagnino M, Brooks AE, Oslapas AN, Gardner KL and Arnoczky SP (2017). Crimp length decreases in lax tendons due to cytoskeletal tension, but is restored with tensional homeostasis. J. Ortho. Res 35: 573–579.

Lee CH, Shin HJ, Cho IH, Kang YM, Kim IA, Park KD and Shin JW (2005). Nanofiber alignment and direction of mechanical strain affect the ECM production of human ACL fibroblast. Biomaterials 26: 1261–1270. [PubMed: 15475056]

Lin J, Kennedy SH, Svarovsky T, Rogers J, Kemnitz JW, Xu A and Zondervan KT (2009). High-quality genomic DNA extraction from formalin-fixed and paraffin-embedded samples deparaffinized using mineral oil. Anal. Biochem 395: 265–267. [PubMed: 19698695]

Liu Y, Keikhosravi A, Mehta GS, Drifka CR and Eliceiri KW (2017). Methods for Quantifying Fibrillar Collagen Alignment. Methods Mol Biol 1627: 429–451. [PubMed: 28836218]

Montes GS and Junqueira LC (1991). The use of the Picrosirius-polarization method for the study of the biopathology of collagen. Mem. Inst. Oswaldo Cruz 86 Suppl. 3: 1–11.

Mueller C, Edmiston KH, Carpenter C, Gaffney E, Ryan C, Ward R, White S, Memeo L, Colarossi C, Petricoin EF, Liotta LA and Espina V (2011). One-step preservation of phosphoproteins and tissue morphology at room temperature for diagnostic and research specimens. PLoS ONE 6.

Muthusubramaniam L, Peng L, Zaitseva T, Paukshto M, Martin GR and Desai TA (2012). Collagen fibril diameter and alignment promote the quiescent keratocyte phenotype. J Biomed. Mater. Res. Part A 100: 613–621.

Neumeister VM (2014). Tools to assess tissue quality. Clin. Biochem 47: 280–287. [PubMed: 24565988]

Pena A, Fabre A, Debarre D, Marchal-Somme J, Crestani B, Martin J, Beaurepaire E and Schanne-Klein M-C (2007). Three-dimensional investigation and scoring of extracellular matrix remodeling during lung fibrosis using multiphoton microscopy. Microsc. Res. Tech 70: 162–170. [PubMed: 17177275]

Provenzano PP, Eliceiri KW, Campbell JM, Inman DR, White JG and Keely PJ (2006). Collagen reorganization at the tumor-stromal interface facilitates local invasion. BMC Med 4: 38. [PubMed: 17190588]

Provenzano PP, Inman DR, Eliceiri KW, Knittel JG, Yan L, Rueden CT, White JG and Keely PJ (2008). Collagen density promotes mammary tumor initiation and progression. BMC Med 6: 11. [PubMed: 18442412]

Puchtler H, Waldrop FS and Valentine LS (1973). Polarization microscopic studies of connective tissue stained with picro-sirius red FBA. Bietr. Pathol 150: 174–187.

Rich L and Whittaker P (2005). Collagen and picrosirius red staining : a polarized light assessment of fibrillar hue and spatial distribution. Braz. J. Morphol. Sci 22: 97–104.

Riching KM, Cox BL, Salick MR, Pehlke C, Riching AS, Ponik SM, Bass BR, Crone WC, Jiang Y, Weaver AM, Eliceiri KW and Keely PJ (2014). 3D collagen alignment limits protrusions to enhance breast cancer cell persistence. Biophy. J 107: 2546–2558.

Sacks MS, Smith DB and Hiester ED (1998). The aortic valve microstructure: Effects of transvalvular pressure. J. Biomed. Mater. Res 41: 131–141. [PubMed: 9641633]

Schenke-Layland K, Xie J, Heydarkhan-Hagvall S, Hamm-Alvarez SF, Stock UA, Brockbank KGM and MacLellan WR (2007). Optimized preservation of extracellular matrix in cardiac tissues: implications for long-term graft durability. Ann. Thor. Surg 83: 1641–1650.

Schindelin J, Rueden CT, Hiner MC and Eliceiri KW (2015). The Image J ecosystem: an open platform for biomedical image analysis. Mol Reprod Dev 82: 518–529. [PubMed: 26153368]

Schoen FJ and Gotlieb AI (2016). Heart valve health, disease, replacement, and repair: A 25-year cardiovascular pathology perspective. Cardiovasc. Pathol 25: 341–352. [PubMed: 27242130]

Sherker AR, Cherepanov V, Alvandi Z, Ramos R and Feld JJ (2013). Optimal preservation of liver biopsy samples for downstream translational applications. Hepatol. Int 7: 758–766. [PubMed: 26201811]

Shirani J, Pick R, Roberts WC and Maron BJ (2000). Morphology and significance of the left ventricular collagen network in young patients with hypertrophic cardiomyopathy and sudden cardiac death. J. Am. Coll. Cardiol 35: 36–44. [PubMed: 10636256]

Staff S, Kujala P, Karhu R, Rökman A, Ilvesaro J, Kares S and Isola J (2013). Preservation of nucleic acids and tissue morphology in paraffin-embedded clinical samples: comparison of five molecular fixatives. J. Clin. Pathol 66: 807–810. [PubMed: 23750036]

Ja Stella and Sacks MS (2007). On the biaxial mechanical properties of the layers of the aortic valve leaflet. J. Biomech. Eng 129: 757–766. [PubMed: 17887902]

Su JMF, Perlaky L, Li X-N, Leung H-CE, Antalffy B, Armstrong D and Lau CC (2004). Comparison of ethanol versus formalin fixation on preservation of histology and RNA in laser capture microdissected brain tissues. Brain Pathol 14: 175–182. [PubMed: 15193030]

von Ahlfen S, Missel A, Bendrat K and Schlumpberger M (2007). Determinants of RNA quality from FFPE samples. PLoS ONE 2: 1–7.

Williams C, Pontén F, Moberg C, Söderkvist P, Uhlén M, Pontén J, Sitbon G and Lundeberg J (1999). A high frequency of sequence alterations is due to formalin fixation of archival specimens. Am. J. Pathol 155: 1467–1471. [PubMed: 10550302]

Williams RM, Zipfel WR and Webb WW (2005). Interpreting second-harmonic generation images of collagen I fibrils. Biophys. J 88: 1377–1386. [PubMed: 15533922]

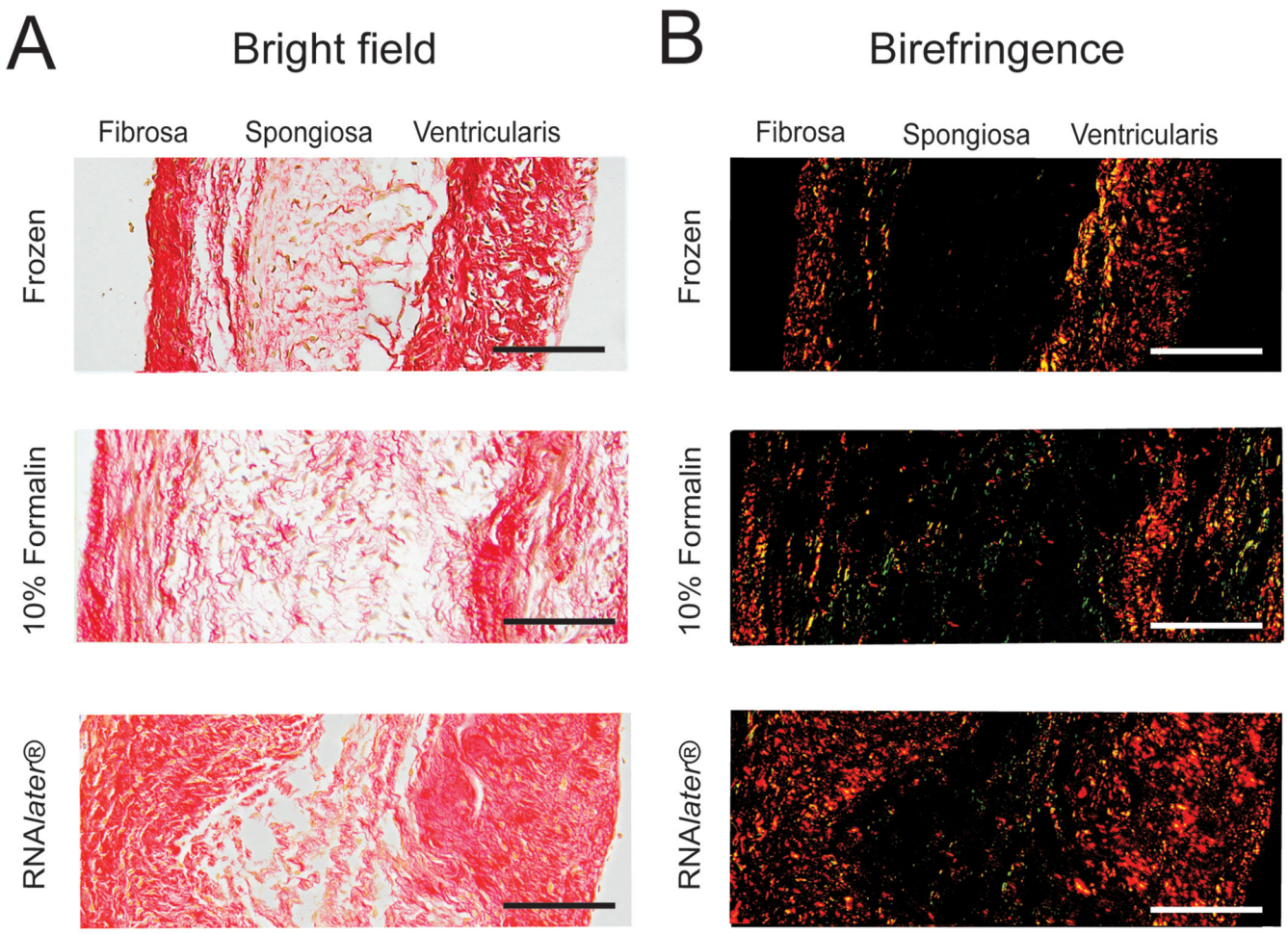

Figure 1.

Collagen in aortic valve leaflets stained with picrosirius red taken using bright field or polarized light (birefringence). Samples were preserved using flash freezing, formalin or RNA*later®*. Scale bar = 50 μm.

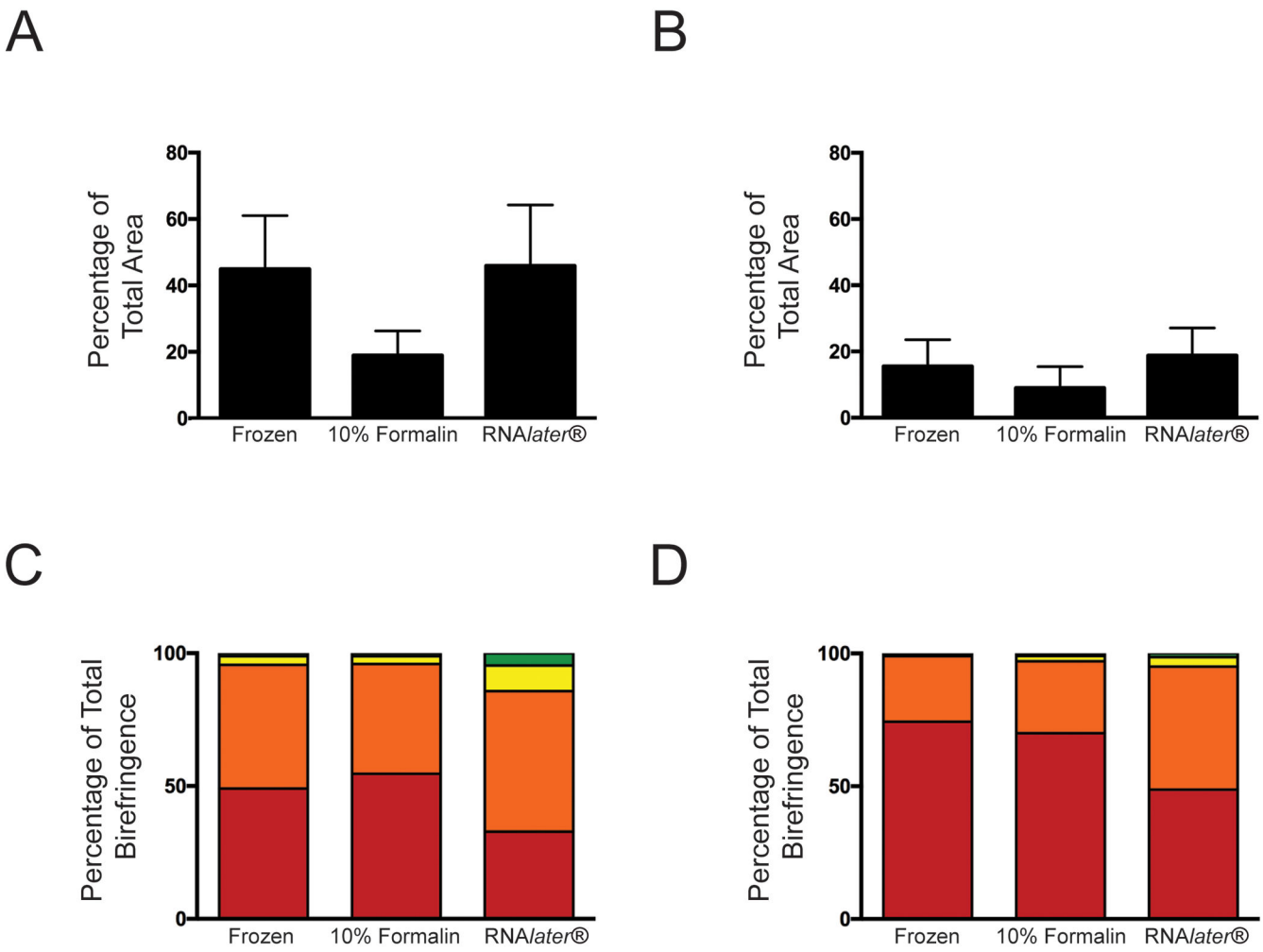

Figure 2.

Quantification of birefringence measured in aortic valve leaflets stained with picrosirius red showing birefringence as a measure of total area within the fibrosa (A) and spongiosa (B). Color of birefringence as a percentage of total birefringence in the fibrosa (C) and spongiosa (D). Red refers to red birefringence (bottom), followed by orange, yellow and green.

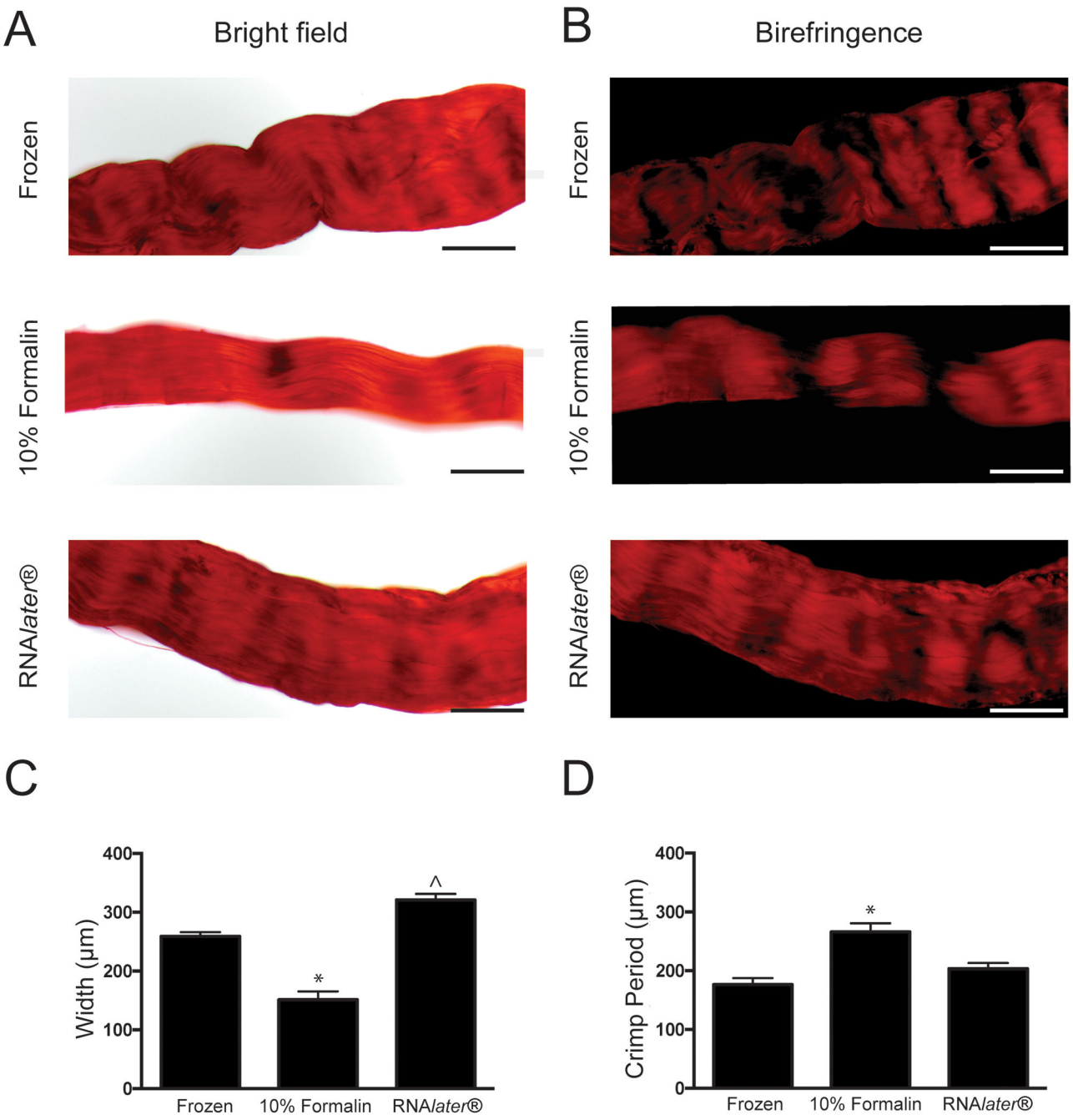

Figure 3.

Visualization and quantification of collagen crimp and fascicle width in RTTfs. RTTfs stained with picrosirius red using bright field (A) or polarized light (B). Scale bar = 200 µm. Quantification of RTTf width (C) and period of collagen crimp (D). *$p < 0.05$ compared to flash frozen. ^$p < 0.05$ compared to formalin. Samples were preserved using flash freezing, formalin or RNA*later®*.

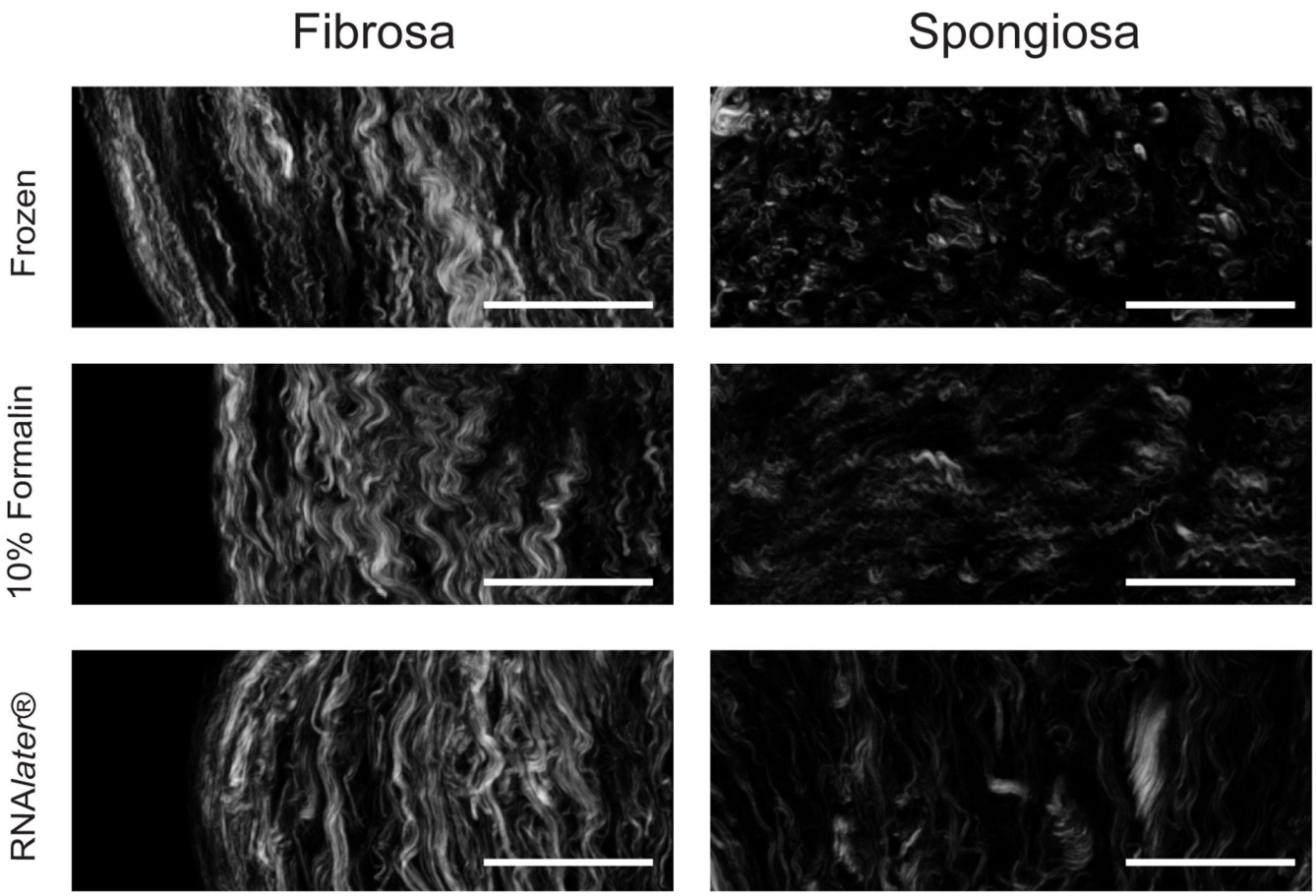

Figure 4.
Collagen in the fibrosa and spongiosa of aortic valve leaflets using SHG imaging. Samples were preserved using flash freezing, formalin or RNA*later*®. Scale bar = 50 μm.

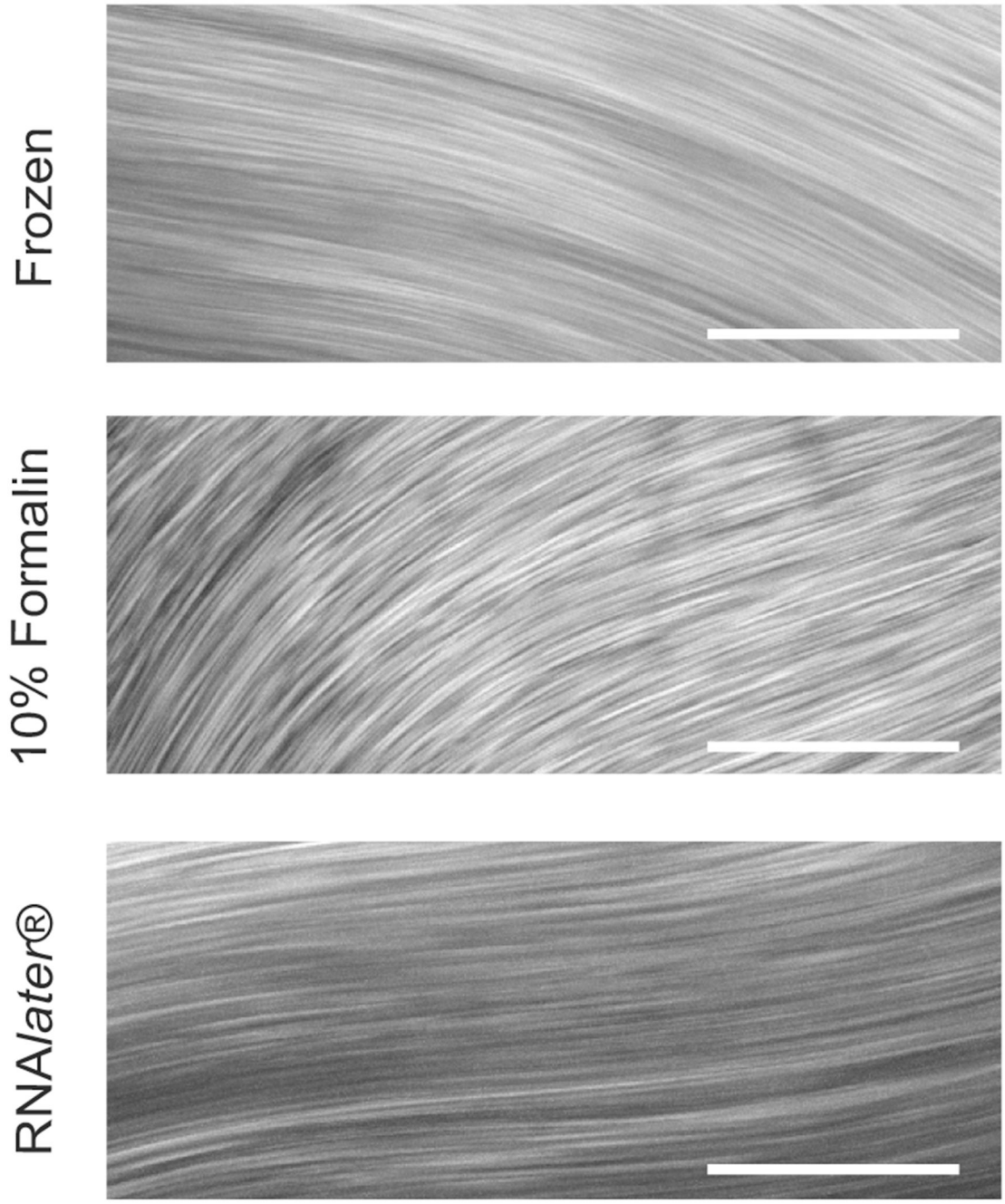

Figure 5.
Collagen fibers in RTTfs using SHG imaging. Samples were using flash freezing, formalin or RNA*later*®. Scale bar = 50 μm.

Table 1.

Collagen fiber architecture in the heart valve leaflet fibrosa

Measurement	Frozen average	10% Formalin average	RNA*later*® average
Fiber dimensions			
Fiber width (μm)	1.91 ± 0.0177	1.91 ± 0.0985	1.89 ± 0.0217
Fiber density			
Distance to nearest 2	6.24 ± 0.517	6.65 ± 1.88	6.06 ± 0.261
Distance to nearest 4	8.75 ± 0.760	9.57 ± 2.87	8.53 ± 0.541
Distance to nearest 8	13.3 ± 1.54	14.7 ± 3.73	12.9 ± 1.02
Distance to nearest 16	20.8 ± 2.96	22.8 ± 5.36	20.2 ± 1.42
Box density 11.25 × 11.25 μm	2.83 ± 0.224	2.66 ± 0.368	2.79 ± 0.153
Box density 22.5 × 22.5 μm	6.07 ± 0.951	5.18 ± 0.890	5.91 ± 0.831
Box density 45 × 45 μm	14.0 ± 2.12	12.4 ± 2.29	13.4 ± 1.83
Fiber alignment			
Fiber absolute angle (°)	77.6 ± 6.17	95.6 ± 7.50[a]	54.3 ± 5.38[a]
Alignment of nearest 2	0.952 ± 0.0449	0.960 ± 0.0293	0.983 ± 0.00519
Alignment of nearest 4	0.922 ± 0.0648	0.927 ± 0.0578	0.969 ± 0.0105
Alignment of nearest 8	0.887 ± 0.104	0.904 ± 0.0623	0.957 ± 0.00943
Alignment of nearest 16	0.835 ± 0.182	0.892 ± 0.0820	0.937 ± 0.0242
Box alignment 11.25 × 11.25 μm	0.987 ± 0.0100	0.990 ± 0.00436	0.992 ± 0.00273
Box alignment 22.5 × 22.5 μm	0.965 ± 0.0230	0.959 ± 0.0221	0.980 ± 0.00869
Box alignment 45 × 45 μm	0.911 ± 0.0847	0.925 ± 0.0517	0.959 ± 0.00475

[a] $p < 0.5$ compared to flash freezing,

[b] $p < 0.5$ compared to formalin fixation.

Table 2.

Collagen fiber architecture in the heart valve leaflet spongiosa

Measurement	Frozen average	10% Formalin average	RNA*later*® average
Fiber dimensions			
Fiber width (μm)	1.89 ± 0.118	1.85 ± 0.0597	1.87 ± 0.0336
Fiber density			
Distance to nearest 2	7.86 ± 0.282	9.62 ± 0.773[a]	8.40 ± 0.370
Distance to nearest 4	12.3 ± 0.600	16.1 ± 1.33[a]	13.0 ± 0.416[b]
Distance to nearest 8	18.9 ± 1.13	25.4 ± 3.08[a]	20.3 ± 1.13
Distance to nearest 16	29.9 ± 1.48	43.0 ± 6.74[a]	33.1 ± 3.10
Box density 11.25 × 11.25 μm	2.55 ± 0.0910	2.52 ± 0.0687	2.42 ± 0.251
Box density 22.5 × 22.5 μm	4.53 ± 0.364	4.24 ± 0.291	4.33 ± 0.661
Box density 45 × 45 μm	8.80 ± 0.269	8.00 ± 0.572	8.02 ± 0.962
Fiber alignment			
Fiber absolute angle (°)	75.2 ± 8.07	92.4 ± 9.72	57.6 ± 7.10[b]
Alignment of nearest 2	0.945 ± 0.0123	0.896 ± 0.0508	0.918 ± 0.00602[a]
Alignment of nearest 4	0.898 ± 0.00985	0.804 ± 0.0450[a]	0.864 ± 0.0185[a,b]
Alignment of nearest 8	0.864 ± 0.00993	0.671 ± 0.0260[a]	0.805 ± 0.0237[a,b]
Alignment of nearest 16	0.806 ± 0.0237	0.601 ± 0.0417[a]	0.764 ± 0.0379[a,b]
Box alignment 11.25 × 11.25 μm	0.989 ± 0.00707	0.966 ± 0.0190	0.977 ± 0.00734
Box alignment 22.5 × 22.5 μm	0.953 ± 0.0189	0.889 ± 0.0203[a]	0.934 ± 0.0309[b]
Box alignment 45 × 45 μm	0.907 ± 0.0158	0.790 ± 0.0317[a]	0.850 ± 0.0196[a]

[a] $p < 0.05$ compared to flash freezing,

[b] $p < 0.05$ compared to formalin fixation.

Table 3.

Collagen fiber architecture in rat tail tendons

Measurement	Frozen average	10% Formalin average	RNA*later*® average
Fiber dimensions			
Fiber width (μm)	1.55 ± 0.0655	1.67 ± 0.0808	1.55 ± 0.0654
Fiber density			
Distance to nearest 2	7.50 ± 1.51	6.86 ± 1.58	6.84 ± 0.427
Distance to nearest 4	11.7 ± 2.58	9.72 ± 2.21	9.69 ± 0.705
Distance to nearest 8	28.3 ± 5.60	23.1 ± 9.74	22.0 ± 1.58
Box density 11.25 × 11.25 μm	2.56 ± 0.265	2.85 ± 0.429	2.84 ± 0.436
Box density 22.5 × 22.5 μm	4.29 ± 0.413	5.71 ± 1.36	5.82 ± 1.31
Box density 45 × 45 μm	8.63 ± 1.88	14.5 ± 5.33	15.5 ± 3.67
Fiber alignment			
Fiber absolute angle (°)	85.6 ± 62.9	58.0 ± 71.9	36.6 ± 15.1
Alignment of nearest 2	$0.999 \pm 9.05 \times 10^{-4}$	0.997 ± 0.00335	0.997 ± 0.00127
Alignment of nearest 4	0.997 ± 0.00152	0.996 ± 0.00222	0.994 ± 0.00259
Box alignment 11.25 × 11.25 μm	$1.00 \pm 6.44 \times 10^{-5}$	$0.999 \pm 8.73 \times 10^{-4}$	$1.00 \pm 1.44 \times 10^{-4}$
Box alignment 22.5 × 22.5 μm	$1.00 \pm 1.59 \times 10^{-4}$	1.00 ± 0.00120	1.00 ± 0.000187
Box alignment 45 × 45 μm	$0.998 \pm 8.29 \times 10^{-4}$	0.996 ± 0.00249	0.996 ± 0.00260

[a] $p < 0.05$ compared to flash freezing

[b] $p < 0.05$ compared to formalin fixation.